Journal of Ceramic Processing Research. Vol. 5, No. 2, pp. 157~162 (2004)

J O U R N A L O F
Ceramic Processing Research

Synthesis of nanostructured carbonated calcium hydroxyapatite by ultrasonic spray pyrolysis

V. Jokanović*, I. Nikčević, B. Dačić[a] and D. Uskoković

Institute of Technical Sciences of the Serbian Academy of Sciences and Arts, Knez Mihailova 35/IV, 11 000 Belgrade, Serbia and Montenegro

[a]Auckland University of Technology, Auckland, New Zealand

Synthesis of high purity submicrometeric spherical particles are of considerable interest for a wide variety of applications, ranging from electronics via ceramics, catalysts to bioceramic due to their unique properties that are primary determined by size, composition and structure. In this paper, the synthesis of carbonate calcium hydroxyapatite by a spray pyrolysis process in an ultrasonic periodical physical field is analyzed. The formation mechanism of aerosol droplets is discussed and the particle size is derived on the assumption that the aerosol droplet represents a mechanical oscillator exited by complex waves which propagate inside the reactor. The particle size distribution is analyzed considering the degeneration of the forced frequency of the ultrasonic oscillator in those complex waves. The phase composition, structure and substructure so obtained of calcium hydroxyapatite particles are investigated by using X-ray diffraction (XRD), infrared spectroscopy (IR) and scanning electron microscopy (SEM) analysis. A fully agreement between the theoretical predicted discrete values for structure and substructure elements (particles and subparticles) and their population balances and experimental values obtained by SEM measurements was found. From that reason, it was evidently confirmed that the process of aerosol/powder particle synthesis can be regarded as a deterministic process.

Key words: calcium hydroxyapatite, ultrasonic spray pyrolysis, structure, substructure, modelling/designing.

Introduction

Ultrasonic spray pyrolysis is a very useful method for the production of nanostructured highly spherical particles with a very narrow size distribution, and high chemical and phase homogeneity. A wide spectrum of materials, which can be synthesized by spray pyrolysis, emphasizes that this method is advantageous compared to other chemical methods of synthesis [1-5]. Modeling of the spray pyrolysis process is given in the literature [5-9] especially for a two-fluid atomizer [6-8].

Aerosol formation in an ultrasonic field related to the genesis and the geometrical characteristics of the synthesized particles was thoroughly described for the first time by a theoretical model [10, 11, 13]. The model defines all obtainable discrete diameters of the particles and their frequencies in the aerosol pyrolysis. Thus, this model allows the foreseeing of the particle size distribution within a given system of sonic spraying enabling, also, the designing of sub-particles size [12].

Calcium hydroxyapatite is a potentially very important material in human medicine as in terms composition and functional properties of its carbonate form, it is very similar to those of bones. Because of the biocompatibility, osteoconductivity and bioresorbility of the carbonate form of CaHAp, calcium hydroxyapatite is used for bone reparation and bone replacement. As the ratio of the carbonate phase increases in the CaHAp so does the surface activity and solubility of the CaHAp in the biological fabric of bone, thereby contributing greatly to the activity of CaHAp at the interface with the bone [14-16].

Several methods for CaHAp synthesis are known today; icluding conventional precipitation from solution [17-19], activated hydrothermal precipitation [20-23], a mechanochemical synthesis method [24-27], a two-stage process with hydrothermal precipitation in the first and mechanochemical treatment in the second stage [28], and a sol-gel reaction from partially hydrolyzed metal organic precursor of phosphorus and calcium soluted in methyl alcohol [29].

This paper elaborates on the thermal synthesis of CaHAp facilitated by ultrasound aerosol spraying of the pre-conditioned precursor solution. There are two reasons why this technique was used. Firstly, the reaction method gives a product with well-controlled average particle size, and consistency in particle and sub-particle size distributions. Secondly, the attainable consistency in the characteristics of the reaction product obtained permits the testing of a theoretical method [10-13] developed for the determination of the particle size, at

*Corresponding author:
Tel : 38111636994
Fax: 38111185263
E-mail: vukoman@itn.sanu.ac.yu or vukomanj@ptt.yu

both the particle and sub-particle levels. Therefore by engineering the periodical physical field we are able to assess how and to what extent the applied field influences the genesis of a particle as well as the structural and substructural characteristics of the synthesized powders.

Experimental Method

Powder synthesis

A water solution of $Ca(NO_3)_2 \times 4H_2O$ and $(NH_4)_2HPO_4$ in estimated molar ratio, which meets the required stoichiometric of CaHAp was the precursor for synthesis. Concentrated nitric acid was used to suppress the precipitation of calcium phosphate from the solution, and to maintain a homogeneous composition of ionic species in the precursor solution. A small quantity of urea was also added for the final conditioning of the feeding solution.

An ultrasonic atomizer (Gapusol 9001, RBI), using a transducer working at 1.7 MHz, was used to spray the feeding precursor solution. The aerosol produced entered the quartz tube (*Heraues Rof 7/50*) and was carried at 1000°C, by nitrogen gas (0.66l s^{-1}). The residence time of aerosol droplets in the reaction cell was 90 s, assuming the nitrogen flow rate and droplet velocities to be equal. The solidified particles carried through the reaction tube settled down in the precipitation compartment. The precipitated powder was composed of "large" blocks of primary particles that we will henceforth address as the secondary particles.

Powder characterization

A scanning electron microscope, (SEM JEOL 5300) equipped with a semiautomatic image analyzer (Videoplan, Kontron), has been used to analyze the distribution of secondary particles.

An X-ray diffraction (XRD) method, (Philips PW 1050), with Cu-$K\alpha_{1-2}$ radiation, was used for phase analysis of CaHAp and determination of the crystallite size and lattice parameters. The average crystallite size was calculated using Sherrer's formula. Infrared Spectroscopy, IR (PERKIN ELMER 983G), with a KBr pastille covering the wave numbers ranging from 400 to 4,000 cm^{-1} was used for phase analysis as well.

Theoretical Models for Structure and Substructure Design of the Particles

Theoretical model for structure design

We have used a theoretical 3D model for the capillary standing waves (which occur at the meniscus of the liquid surface), whose detailed analysis is given in referencies [10, 11, 13], and have been used for evaluation of the expression for the average diameter of an aerosol droplet (d_{da}) created by means of the ultrasonic oscillator:

$$d_{da}=\left(\frac{\pi\sigma}{\rho f^2}\right)^{\frac{1}{3}} \tag{1}$$

where σ is the surface tension of the solution, ρ - the solution density, and f - the frequency of the ultrasonic generator.

Assuming that the discrepancy among the values for damping factors for transverse and longitudinal waves is significant, if the thickness of the liquid column is not insignificant, than it is necessary to make the applied theoretical model more precise by introducing an appropriate damping factor. The damping factor is needed due to different speeds of the wave propagation alongside the lamellar fluid layers and in a direction orthogonal to this wave pathway [11, 13]. Therefore, there is not obtained only one discrete value is obtained, which corresponds to the spherical form of the standing wave. Instead, because of degeneration of the standing wave, a spectrum of discrete values for the diameter of aerosol droplet is obtained:

$$d_d=\frac{1}{\pi}\left(\frac{2\sigma\pi}{\rho f^2}\right)^{\frac{1}{3}}[1(l-1)(l+2)]^{\frac{1}{3}} \tag{2}$$

where: l is an integer, which takes values $1 \geq 2$.

On the other hand, the disturbance caused by the forced frequency of the ultrasonic oscillator on the liquid precursor renders an innate oscillation within the column of the liquid precursor, which is in accordance with the shape and the physical properties of the liquid phase. As a result, an additional disturbance of the frequency of the ultrasonic oscillator takes place. This is tuned to the values that themselves include the resulting correction innate to the underlying damping factor, which is caused by changing the shape of the standing waves and, also, by the characteristics of the induced mechanical oscillator in the liquid column, which in turn is influenced by the width of the liquid column $\boldsymbol{h}$ and by the speed of the ultrasonic propagation $\boldsymbol{c}$ through the liquid column [11]. The distribution spectra for the diameters of aerosol droplets, which satisfy the effects of both factors for the frequency degeneration of the forced oscillator, can be obtained from the following expression:

$$d_d=\left[\frac{\pi\sigma}{\rho p^2 c^2/4h^2}\right]\left[\frac{(2l(l-1)(l+2))^{\frac{1}{3}}}{\pi}\right] \tag{3}$$

The discrete values for the diameter of aerosol droplets, in the distribution spectrum, have been further related to the solid particle size by applying the pertinent mass reduction factor due to the solidification and pyrolysis processes involved [5, 9-13]:

$$d_p = d_d \left(\frac{c_{pr} M_p}{\rho_p M_{pr}} \right)^{\frac{1}{3}} \quad (4)$$

where: d_p is diameter of a powder particle, ρ_p- the powder density, M_p- molecular mass of the powder, c_{pr}- concentration of the precursor solution, and M_{pr}- molecular mass of the precursor.

Designing the substructure of particles

After separation of an aerosol droplet from the surface at the liquid meniscus, the droplet still remains in an activated state inherited at the very moment it was born. Such an aerosol droplet behaves as an induced mechanical oscillator, the innate frequency of which depends on the geometry of the droplet (induced frequency is the frequency at the moment of droplet separation from the meniscus). The diameter of a nano-droplet, which forms the sub-structure of an aerosol droplet, can be determined by using the 3D model for the standing wave (with central symmetry) generated as the result of the excitation transmitted from the ultrasonic generator to the droplet, which is discussed in detail in Ref 12:

$$D_{sd} = \frac{Nc}{f} \quad (5)$$

where $\boldsymbol{D_{sd}}$ is the diameter of a sub-droplet, *c*- the ultrasonic speed and *f*- frequency of the ultrasonic oscillator. The numerical constant N takes different values for different solutions of the standing wave equation, dependently on the morphology of sub-droplets, i.e., on the deformation of their spherical shapes.

The particle size distributions

The particle size distribution in the synthesized powder can be estimated from the following equation [12]:

$$I_{10} : I_{20} : I_{30} : \ldots : I_{n0} = \frac{1}{\Delta f_1} : \frac{1}{\Delta f_2} : \frac{1}{\Delta f_3} : \ldots : \frac{1}{\Delta f_n}, \quad (6)$$

This equation was evaluated on the basis of frequencies of the appearance of discrete particle sizes in the synthesized product [11] in the distribution spectrum found. The I_{10}, I_{20}, I_{30}, and I_{n0} intensities are frequencies for the corresponding discrete particle diameters, and Δf_1, Δf_2, Δf_3, and Δf_n are displacements of the real frequencies (the appropriate discrete values for particles diameters) from the initiation frequency produced by the ultrasonic generator. The relative ratios of intensity - the frequency of a particular diameter - if normalized provides the basic relationship for calculation of the absolute value for the intensity:

$$I_{10} + I_{20} + I_{30} + \ldots + I_{n0} = 1 \quad (7)$$

Results and Discussion

Characterization of CaAHp particles

X-ray diffraction

X-ray diffraction analysis in Fig. 1 shows all the characteristic peaks are present in the synthesized powder. Also, the obtained relative intensity for all characteristic diffraction maxima - (211) I_{100}, (112) I_{60}, (300) I_{60}, (002) I_{40}, (213) I_{40}, (222) I_{30}, (202) I_{25}, (004) I_{20} i (210) I_{18} - correspond to the relative intensities of diffraction maxima found on a standard sample (JCPDS No. 9-432) [30-33].

When Sherrer's formula for calculating the crystallite size was applied, a size of 13 nm was found for the CaHAp crystallites. Calculated lattice parameters are c=0.6885 nm and a=0.9460 nm. These values are close to the standards values for CaHAp; c=0.6884 nm and a =0.9386 nm [33], and the differences that appeared are small.

IR Spectroscopy

The IR spectrogram in Fig. 2 shows all the charac-

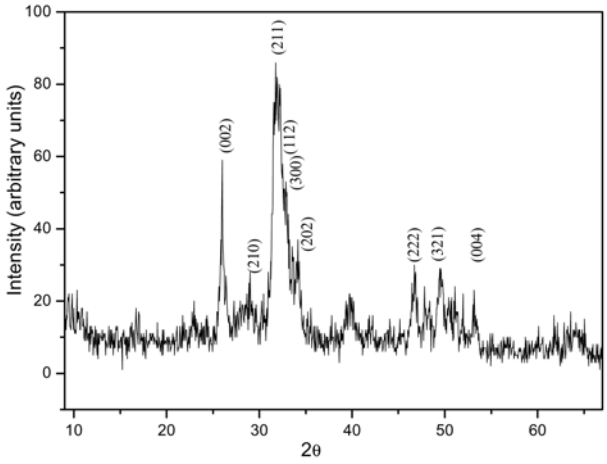

Fig. 1. X-ray diffraction of the CaHAp powder.

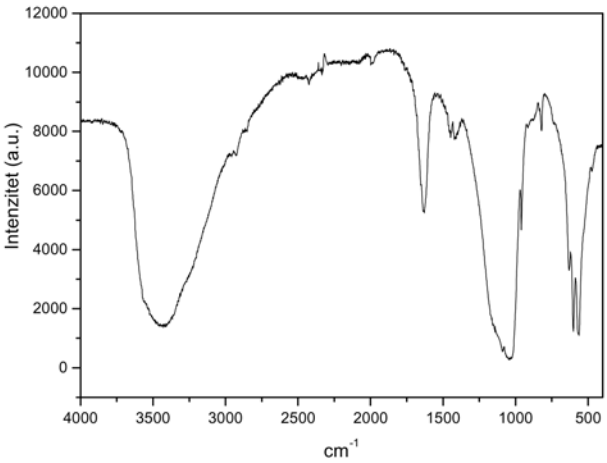

Fig. 2. IR spectrogram of the CaHAp powder.

Table 1. Distribution of the measured particles sizes

Vol. parts, I_n	0.085	0.21	0.32	0.21	0.02	0.11	0.02	0.04
d_p, nm	405	497	554	612	653	708	811	909

teristic bands for hydroxyapatite [30, 34-35]. The asymmetrical stretching (ν_3) and bending (ν_4) modes of PO_4^{3-} ion were detected at around 1092 and 1042, and 603 and 569 cm^{-1}, respectively. The symmetrical stretching modes (ν_1 and ν_2) of PO_4^{3-} ion were also found at around 957 and 473 cm^{-1}. The liberation and stretching mode of the OH^- were detected at around 630 cm^{-1} and 1626 cm^{-1}, respectively. The stretching vibrations ascribed to CO_3^{2-} at around 1442, 1406 and 875 cm^{-1} are present, also. This indicates that the carbonate group is incorporated in the apatite structure.

Designing the particle size

The average particle diameter of synthesized CaHAp was obtained by a numerical procedure, (equations (6) and (7)), which takes in to account the discrete diameters of the particles, as well as theirs ratios taken from the experimental distribution curve (Table 1 and Fig. 3).

The average particle diameter of 572 nm was obtained by counting the number of particles that have the same discrete values for diameter that are given in Table 1.

A similar approach has been made for the theoretically predicted particle size distribution using the equations (2) and (4) that allow the calculation of the discrete particle sizes and equations (6) and (7) that give the corresponding discrete ratios values in the total particle size distributions. The theoretical model applied

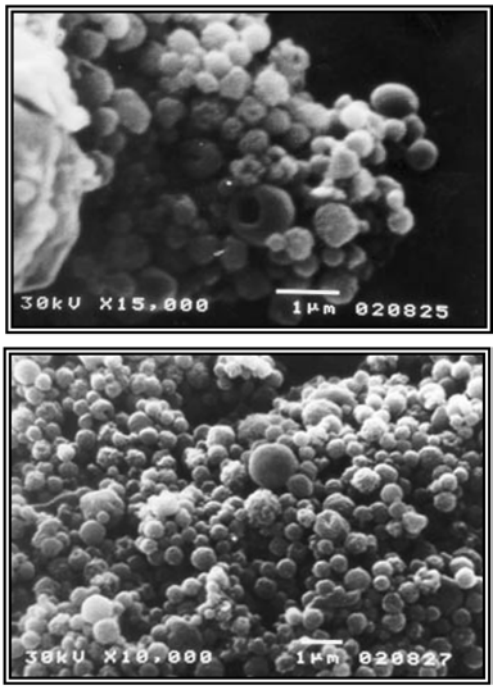

Fig. 3. SEM microphotographs of CaHAp powder.

to the droplet distribution assessment (equations (3) and (4)) encompasses all the discrete diameters for aerosol droplets in Table 2. These values are between 2.1 and 6.7 μm. The average diameter of the aerosol droplet is 3.2 μm. This span of discrete values is the consequence of deformation of the 3D standing waves by the affect of the damping factor caused by the depth of the liquid column which is imposed on the effect of the ultarasonic generator.

By applying equation (4), which defines the decrease of particle size during the solidification stage of the synthesis process, caused by CaHAp precipitation, drying, and phase transformation, the discrete values for the particle diameter can be obtained. These values are within the interval 360 to 1144 nm, which is pertinent to the frequencies that take values between 4.78 and 0.84 MHz. Since the experimental study was done with a depth of the liquid column, which is considerably less than the other two dimensions are (h=4 mm, a=b=5 cm), a narrow distribution for the discrete values of the aerosol droplets was obtained, as expected. Hence, a narrow distribution of the solid particle sizes was also obtained. As a matter of fact, almost 80 per cent of all particles were 558 nm in diameter.

The average particle diameter for CaHAp estimated by the theoretical model employed with equations (6) and (7) has a value of 573.4 nm, which is in excellent agreement with the experimentally obtained value of 572 nm. If we look at the discrete values for diameters in the theoretical particle size distribution and compare them with the distribution of experimentally measured diameters of particles, it can be elucidated that in both cases the distributions are very narrow, within approximately the same interval; 497-612 nm in the spectrum of measured diameters, and 459-737 nm in the spectrum of theoretically estimated diameters. The 554 nm particles have a maximum fraction in the experimentally determined distribution, while the maximum ratio in the theoretically anticipated distribution has particles 558 nm in diameter.

Assessments accomplished by the analytical model allow an estimation of other characteristic parameters for the system of CaHAp powder synthesis such as the frequency of droplet creation with a particular diameter, as well as for the shift of this frequency created from the initial frequency produced by the ultrasonic generator. These values are shown in Table 2.

Table 2. Parameters of theoretically predicted distribution for the particle sizes

Vol. parts, I_n	0.02	0.06	0.8	0.06	0.03	0.03
d_d, μm	2.1	2.7	3.28	4.3	5.4	6.7
$f_{rez.}$, MHz	4.78	3.74	2.45	1.85	1.16	0.84
$\nabla f_{rez.}$, MHz	2.28	1.24	0.05	0.75	1.34	1.66
d_p, nm	360	459	558	737	916	1144

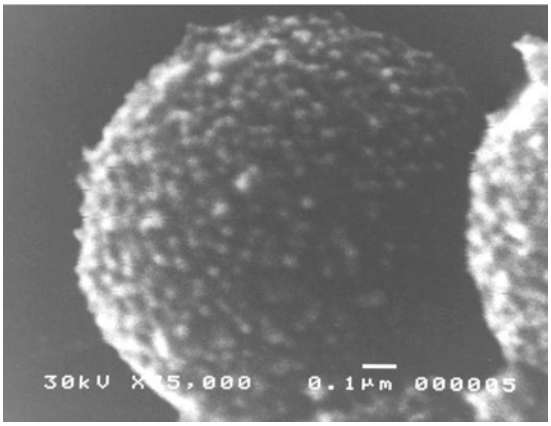

Fig. 4. Typical view of subparticles at the $CaHA_p$ particle surface.

When distribution of the sub-droplets (sub-particles) build up to primary droplets (particles) are considered, under the assumption made that all sub-droplets/particles are alike, while the discrepancies in the primary droplets/particles are insignificant, than the average sub-droplet size (D_{sd}) can be calculated from equation (5), and from there the average diameter of sub-particles (D_{sp}) can be estimated. These values are 76 nm and 12.9 nm, respectively.

It is obvious, as can be seen in the Fig. 4, that the mean subparticle diameter for subparticles at the surface of the particle was about 15 nm. This is in good agreement with calculated values calculated from the above model of the design of subparticles.

Also, the sub-particle diameter obtained from the theoretical model [12] is almost identical to the value of 13 nm obtained by Sherrer's formula from the X-ray diffractogram of the synthesized CaHAp powder. Thus it was found that sub-particles of CaHAp are ordered on the crystallite level.

Conclusions

Analytical modeling and an experimental study of the ultrasonic spray pyrolysis process of CaHAp have been accomplished. It has been found that:

- X-ray phase analysis and IR spectroscopy have shown that the carbonated form of CaHAp was synthesized, with the crystal cell parameters a= 0.964 nm and b=0.688 nm.
- The average particle size of CaAHp obtained by solidification of the aerosol droplets created is 572 nm, while the theoretically predicted value for the average particle diameter is 573 nm.
- A narrow particle size distribution was found showing no significant difference in real size distribution obtained experimentally and theoretically predicted.
- The comparative experimental and analytical studies made have shown that the results obtained are very close, pointing out that the harmonization of the ultrasonic field (or any other periodic physical field to which effect the system would be imposed), define in full the structural characteristics of the system. This is the case at the droplet/particle and sub-droplet/sub-particle level.

Acknowledgements

This work was supported by the Ministry of Science and Technology of the Republic of Serbia through project No. 1431 “Molecular Designing of Monolithic and Composite Materials”. We would like to thank M.Miljkoviæ, Z.Nedic and M. Mitric for their useful experimental support.

Literature

1. A. Lundquist, T.T. Kodaš, D.M. Smith, X. Xiu, S.L. Hietala, and R.T. Paine, J. Am. Ceram. Soc. 74 (1991) 3126-28.
2. O. Milošević, B. Jordović, and D. Uskoković, Mater. Lett. 19 (1994) 165-70.
3. Lj. Ćerović, S. Milonić, Lj. Živković, and D. Uskoković, J. Am. Ceram. Soc. 79[8] (1996) 2215-17.
4. Z.V. Šaponjić, Z. Rakoćević, N.M. Dimitrijević, J.M. Nedeljković, V. Jokanović, and D.P. Uskoković, Nanostract. Mater. 10 (1998) 341-348.
5. G.L. Messing, S.C. Zhang, and G.V. Jayanthi, J. Am. Ceram. Soc. 76 (1993) 2707-2726.
6. F. Iskandar, I.W. Lenggoro, B. Xia, and K.J. Okuyima, Nanopart. Res. 3 (2001a) 263-270.
7. Iskandar, F., Mikrajuddin, Okyuima, K. Nano Lett. 1 (2001b) 231-234.
8. Lefebvre, A.H., Atomization and sprays, Hemisphere, New York, 1989.
9. G.V. Jayanthi, S.C. Zhang, and G.L. Messing, J. Aerosol. Sci. and Techn. 19 (1993) 478-490.
10. V. Jokanović, Dj. Janaćković, A.M. Spasić, and D. Uskoković, Mater. T. JIM 37 (1996) 627-635.
11. V. Jokanović, Dj. Janaćković, and D. Uskoković, Ultrasonic Sonochem. 6 (1999) 157-169.
12. V. Jokanović, Dj. Janaćković, and D. Uskoković, J. Nanostruct. Mater. 12 (1999) 349-352.
13. Dj. Janaćković, V. Jokanović, Lj. Kostić-Gvozdenović, Lj. Živković, and D. Uskoković, J. Mater. Res. 11 (1996) 1706-1716.
14. L.L. Hench, J. Am. Ceram. Soc. 74 (1991) 1487-1510.
15. L.L. Hench, J. Am. Ceram. Soc. 81[7] (1998) 1705-1728.
16. R.Z. LeGeros, J.P. LeGeros, Dense hydroxiapatite. In. L.L. Hench and J. Wilson editors, An introduction to Bioceramics, Adv. Ser. Ceram. 1 (World Scientific Publishing Co. Pte. Ltd., London, Hong Kong, Singapure (1998) 139-180.
17. S.R. Kim, J.H. Lee, Y.T. Kim, D.H. Riu, S.J. Jung, Y.J. Lee, S.C. Chung, and Y.H. Kim, Biomaterials 24 (2003) 1389-1398.
18. S. Lazić, S. Zec, N. Miljević, and S. Milonjić, Termochim. Acta 374 (2001) 13-22.
19. E.G. Nordstrom and K.H. Karlsson, J. Mater. Sci.: Materials in Medicine 1 (1990) 182-184.
20. S. Jinawath, D. Pongkao, W. Suchanek, and M. Yoshimura, Int. J. Inorg. Mater. 3 (2001) 997-1001.

21. H.S. Liu, T.S. Chin, S.Y. Chiu, K.H. Chung, C.S. Chang, and M.T. Lui, Ceram. Int. 23 (1997) 19-25.
22. J. Liu, X. Ye, H. Wang, M. Zhu, B. Wang, and H. Yan, Ceram. Int. (in press).
23. M. Andres-Verges, C. Fernandez-Gonzalez, and M.M. Martinez-Gallego, J. Eur. Ceram. Soc. 18 (1998) 1245-1250.
24. N. Nikčević, V. Jokanović, Z. Nedić, M. Mitrić, and D. Uskoković, J. Solid State Chem. (submitted 2003).
25. K.C.B. Yeong, J. Wang, and S.C. Ng, Biomaterials 22 (2001) 2705-2712.
26. Sang-Hoon Rhee, Biomaterials 23 (2002) 1147-1152.
27. W. Kim, Q. Yhang, and F. Saito, J. Mater. Sci. 35 (2000) 5401-5405.
28. W.L. Suchanek, P. Shuk, K. Byrappa, R.E. Riman, K.S. TenHuisen, and V.F. Janas, Biomaterials 23 (2002) 699-710.
29. K. Cheng, W. Weng, G. Han, P. Du, G. Shen, J. Yang, and J.M.F. Ferreira, Mater. Chem. Phys. 78 (2003) 767-771.
30. R.N. Panda, H.F. Hsieh, R.J. Chung, and T.S. Chin, J. Phys. Chem. Solids 64 (2003) 193-199.
31. H. Rietveld, J. Appl. Crystalog. 2 (1969) 65-71.
32. R.W. Cheary and A.A. Coelho, J. Appl. Crystalog. 25 (1992) 109-121.
33. JCPDS File No. 9-432 (CHA), International Center for Diffraction Data.
34. R.A. Nyquist and R.O. Kagel, Infrared Spectra of Inorganic Compounds, (3800-45 cm^{-1}), Academic Press, New York and London, 1971, 493.
35. K. Nakamoto, Infrared and Raman Spectra and Coordination Compounds, John Wiley and Sons, New York, Chichester, Brisbane, Toronto, 1978.